JEM

*Journal of Electron Microscopy* **61(1)**: 9–15 (2012)
doi: 10.1093/jmicro/dfr078

Physical: Full-length

# Application of theta-scan precession electron diffraction to structure analysis of hydroxyapatite nanopowder

Kyung Song[1,2], Youn-Joong Kim[1,3], Yong-Il Kim[4] and Jin-Gyu Kim[1,*]

[1]Division of Electron Microscopic Research, Korea Basic Science Institute, 113 Gwahangno, Yuseong-gu, Daejeon 305-333, South Korea, [2]Department of Materials Science and Engineering, Pohang University of Science and Technology, Pohang 790-784, South Korea, [3]Graduate School of Analytical Science and Technology, Chungnam National University, 99 Daehak-ro, Yuseong-gu, Daejeon 305-764, South Korea and [4]Korea Research Institute of Standards and Science, 209 Gajeong-ro, Yuseong-gu, Daejeon 305-340, South Korea

*To whom correspondence should be addressed. E-mail: jjintta@kbsi.re.kr

**Abstract** The structure of hydroxyapatite (HA) nanopowder has been determined by theta-scan precession electron diffraction (TS-PED) and Rietveld analysis. To evaluate the usefulness of the TS-PED technique, this result was compared with that of the Rietveld analysis using conventional electron diffraction (ED) and normal precession electron diffraction (PED). The intensity ratios of the (002) to (121) reflections ($I_{002}/I_{121}$) obtained by both PED data were in better agreement with the reference X-ray diffraction (XRD) data than that obtained by the conventional ED data. Although the lattice parameters of HA determined by the TS-PED data were slightly deviated from the reference XRD data, the *a*/*c*-axis ratio had the best agreement with the reference XRD data. The reliability factors ($R_p$, $R_{wp}$ and $\chi^2$) of TS-PED refinement results were substantially improved, when compared with the values obtained by the conventional ED data. These results demonstrate that TS-PED technique could be a useful analytical method for structure determination of nanopowder.

**Keywords** precession electron diffraction, theta-scan technique, nanopowder, Rietveld analysis, hydroxyapatite

**Received** 18 April 2011, accepted 4 October 2011; online 8 December 2011

## Introduction

X-ray crystallography has been well adapted to the structure analysis of large single crystals. However, in the current research trend and application toward nanosized materials, X-ray diffraction (XRD) technique frequently encounters its limitation for structure solution due to insufficient intensity data. From this perspective, electron crystallography could be a powerful tool for structure determination of nanosized materials because of the stronger interaction between electrons and matter than the one observed in X-ray. Electron crystallographic techniques using the conventional electron diffraction (ED) have recently been applied successfully to the nanosized crystalline materials [1–3]. Nevertheless, electron crystallography has some inherent problems, among which the dynamical effects of ED for larger crystalline materials (>50 nm) are the most serious problem for structure solving. As a solution for this problem, the precession electron diffraction (PED) technique turned out to be powerful in obtaining intensities of all reflections closer to the kinematical diffraction conditions [4]. Several crystal structures of advanced materials (such as inorganics, metal alloys, complex oxides and organics) have been solved

and refined using the PED technique [5–11]. However, this technique has been predominantly applied to single crystals and rarely applied to nanopowder. Recently, Prodan and Ciupina [12] reported their results of PED application to polycrystalline materials without a detailed discussion about structure determination and usefulness of the PED technique.

In this study, we tried to determine the crystal structure of hydroxyapatite (HA) nanopowder using different PED techniques. The HA nanopowder, which was used as a test material, has attracted wide interest as a potential structural ceramics for medical implant. The three-dimensional (3D) structure of large HA crystals (>500 nm) was determined using XRD and high-resolution transmission electron microscopy (HRTEM) [13]. For nanosized HA crystals, however, it is difficult to extract 3D structure information using XRD or HRTEM because of their poor crystallinity, structural complexity and sample aggregation [14]. In this study, we have reported the results of the Rietveld analysis of the HA nanopowder and discussed the usefulness of PED techniques for structure determination of nanopowder in general.

## Experimental

### Electron powder diffraction

Material for this study was obtained from a commercial HA nanopowder (ALDRICH, AL574791, 99.999%, metal basis synthetic). The crystal structure of HA, $Ca_5(PO_4)_3(OH)$, has a hexagonal symmetry, $P6_3/m$ (#176), and lattice parameters $a = 9.417(2)$ Å and $c = 6.875(2)$ Å [15] (see the supplementary data online Fig. S1). Samples for electron microscopy were prepared by diluting HA nanopowder in alcohol, and the suspension was dropped on an ultra-thin carbon-supported Cu grid (Ted Pella, Inc.).

Conventional ED and PED patterns were collected using the 2k CCD camera (USC1000, Gatan) on JEM-2100F (JEOL Ltd) operating at 200 kV. All ED patterns were acquired using different exposure times and checked whether the most intense reflection was saturated or not. They were acquired with a nearly parallel incident beam employing the C2 aperture of 10 µm. All PED patterns were obtained at a precession angle of 2.3° with the 'Spinning Star' precession unit (NanoMEGAS Ltd). Theta-scan (TS) PED patterns were obtained by collecting a series of PED patterns with different scattering ranges by controlling the projector shift deflector of the TEM.

The intensity profiles of the conventional ED and PED patterns were extracted using program ELD [16] and analyzed with program FULLPROF [17] for Rietveld analysis [18].

### X-ray powder diffraction

XRD of the HA nanopowder sample was obtained with Dmax2200 (Rigaku Ltd) utilizing graphite-monochromated Cu Kα radiation. The $2\theta$ ranges were from 5° to 140° in the step of 0.02°. The total acquisition time was 24 h, and 7000 data points were collected. The obtained XRD data were subjected to Rietveld analysis using General Structure Analysis System [19].

## Results

### Theta-scan precession electron diffraction

To examine the sample size and distribution, the bright-field TEM image of the HA nanopowder and the corresponding ED pattern was obtained (Fig. 1a). The average size of the HA nanopowder was ~98.6 nm, and the size distribution was shown in Fig. 1b.

For accurate determination of the crystal structure, ED patterns were obtained by several acquisition conditions. In general, small camera length (<250 mm in our TEM) allowed collection of higher order reflections by increasing the field of view of the CCD camera, but it gave rise to overlapping of reflections due to the reduced pixel resolution of the CCD camera. As many $d$-spacings in the HA structure were in close proximity, overlapping of the diffraction peaks was quite severe.

To overcome this problem, ED patterns were acquired by shifting the transmitted beam to the edge of the CCD camera. It brought about an increase in the resolution of ED patterns. For the acquisition of higher pixel resolution and evaluation of precession effects, conventional ED and normal PED patterns were obtained at a camera length of 600 mm which was chosen for the maximum enlargement of the ED pattern with 0.7 Å resolution

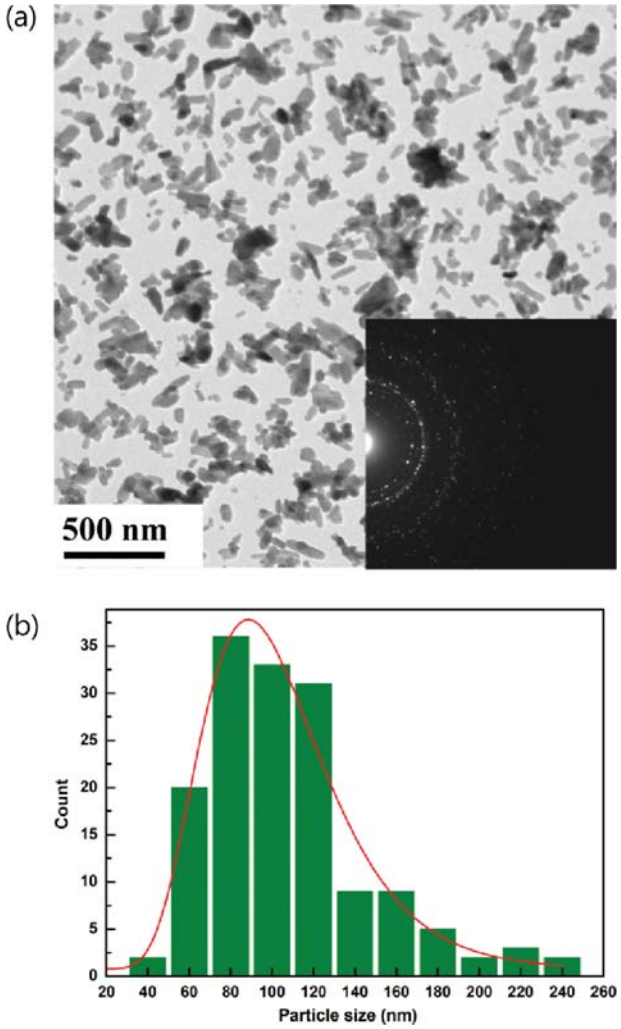


**Fig. 1.** (a) Bright-field TEM image of the HA nanopowder. The corresponding ED pattern was displayed in the inset. (b) Distribution of particle sizes measured from the TEM image and fitted to lognormal function.

inside the 2k CCD as shown in Fig. 2a and b. However, when compared with the experimental XRD data (7000 points), its pixel resolution or data points (2000 points) need to be extended or increased for more reliable structure determination.

To enhance both pixel and resolution of ED patterns, TS-PED patterns were collected (Fig. 2c) at a larger camera length of 1200 mm. To maintain the same resolution as the normal PED pattern, a series of PED patterns with different scattering ranges were obtained by controlling the projector shift deflector. Furthermore, TS-PED patterns were acquired from each range with different exposure times from 5 s to >20 s. In this way, the limited dynamical range of the CCD camera could be compensated such that weak reflections were recorded

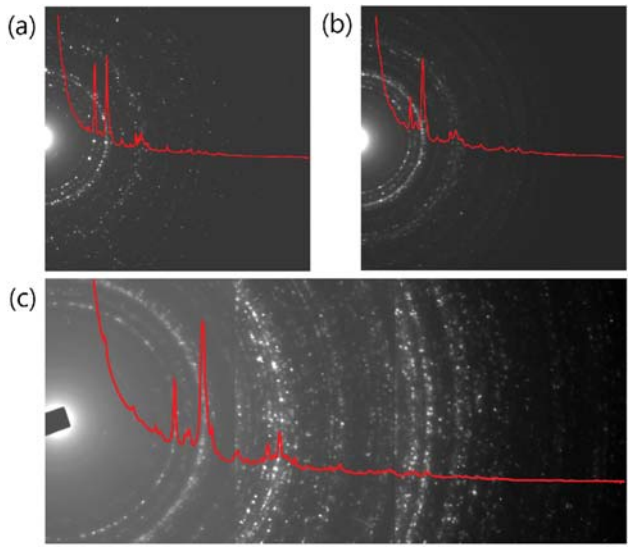


**Fig. 2.** ED patterns of the HA nanopowder: (a) conventional ED pattern, (b) normal PED pattern and (c) TS-PED pattern. The ED patterns in (a) and (b) were recorded with the same camera length of 600 mm for evaluation of precession effects. The TS-PED pattern was recorded at larger camera length of 1200 mm and the theta-scan technique was used to secure the same resolution as other ED patterns. The overlay on the ED shows the average intensity profile that was used to determine the crystal structure. While the conventional ED pattern is marked by severe spotty reflections, the spotty reflections are reduced and become continuous rings in PED patterns.

with longer exposure times, while strong reflections were recorded with shorter exposure times. The intensity profiles of ED patterns were extracted using the ELD application. Thereafter, three intensity profiles were merged to obtain a complete intensity profile by applying the scale factor which was calculated by referring the common reflections in each intensity profile.

The overlay on all ED patterns showed the average intensity profile which was used to determine the HA crystal structure. It could be clearly observed that severe spotty reflections in conventional ED patterns became more continuous and uniform rings in all PED patterns.

### Intensity ratio $I_{002}/I_{121}$

To check the precession effect on the diffracted intensity, we compared the intensity profiles of ED patterns recorded by conventional ED and PED techniques. The *d*-values of the intensity profile were converted to XRD $2\theta$ ranges (Fig. 3). The intensity of the (002) reflection is very important in the HA structure because it usually indicates

texture characteristics of HA nanocrystals in bone and bone-related materials [20–22]. As shown in Fig. 3, the intensity ratio of (002) reflection to (121) reflection $I_{002}/I_{121}$ obtained using PED was more reliable than that obtained using conventional ED.

A more detailed comparison of data quality was presented in Table 1 that showed $I_{002}/I_{121}$ values obtained from the XRD and three different ED data as well as full-width at half-maximum (FWHM) values of the (002) and (121) reflections. It can be noted that the intensity ratio (0.48) measured by the PED data agrees well with the reference XRD data (0.49), when compared with the conventional ED data (0.84). This result clearly demonstrates that PED produces less dynamically affected intensities than the case in conventional ED.

On the other hand, the FWHM values of the (002) and (121) reflections of normal PED did not improve, when compared with those of the conventional ED due to imperfection of the descan alignment of the precession unit and peak overlapping. However, application of TS-PED resulted in substantial improvement in the FWHM value of the (002) reflection from 1.02° to 0.61°.

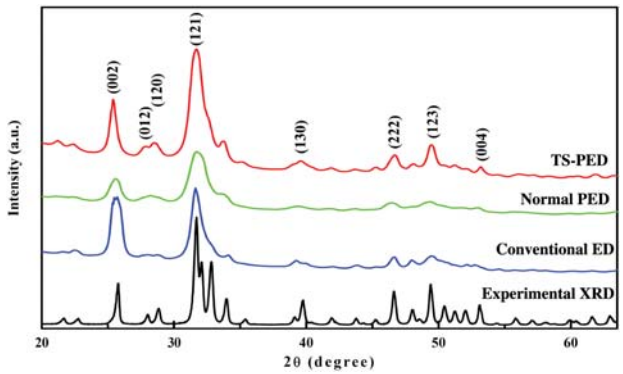


**Fig. 3.** Intensity profiles of experimental XRD data and three different ED data.

**Table 1.** Comparison of the intensity ratio and FWHM values of main reflections derived from three different ED data with those obtained by XRD data

| | Intensity ratio ($I_{(002)}/I_{(121)}$) | FWHM[a] | |
|---|---|---|---|
| | | (002) reflection | (121) reflection |
| XRD (ref.) | 0.49 | – | – |
| XRD (exp.) | 0.39 | 0.29 | 0.36 |
| Conventional ED | 0.84 | 1.02 | 1.08 |
| Normal PED | 0.48 | 1.18 | 1.67 |
| TS-PED | 0.48 | 0.61 | 1.40 |

[a]FWHM determined from Rietveld analysis gives a $2\theta$ peak broadening (in X-ray scattering angle).

### Structure analysis of the HA nanopowder

Rietveld analysis was carried out to obtain structural parameters and reliability factors for all ED data, using the program FULLPROF modified with atomic scattering factors for electrons [23]. Figure 4 shows the result of Rietveld analysis of the TS-PED data. The $d$-values of the intensity profile were converted to $2\theta$ angles for the electron wavelength in this Rietveld analysis process.

To test the usefulness of PED techniques for structure determination, the refinement results of experimental XRD and three different ED data were compared (Table 2). While the refinement of TS-PED data yielded the lattice parameters, $a = 9.264$ Å and $c = 6.775$ Å, which were slightly deviated from the reference XRD data, the $a/c$-axis ratio (1.367) of the lattice parameters determined with the TS-PED data had the best agreement with the reference XRD data. The lattice parameters

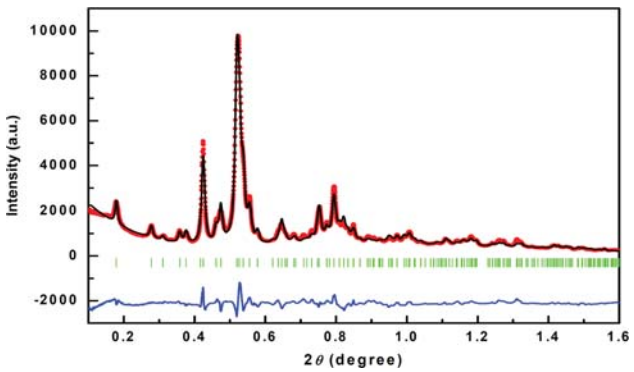


**Fig. 4.** Rietveld analysis result of TS-PED data. The positions of the Bragg reflections were indicated by vertical bars. The difference between the observed intensities (dots) and the calculated intensities (solid line) from the refined model was shown in the lower part of the diagram.

**Table 2.** Results of structure determination derived from three different ED data are compared with those obtained by XRD data

| | Lattice parameters | | | Reliability factors | | | |
|---|---|---|---|---|---|---|---|
| | $a$ (Å) | $C$ (Å) | $a/c$ | $R_p$ (%) | $R_{wp}$ (%) | $R_{exp}$ (%) | $\chi^2$ |
| XRD (ref.) | 9.417(2) | 6.875(2) | 1.370 | – | – | – | – |
| XRD (exp.) | 9.415(2) | 6.882(1) | 1.368 | 6.62 | 8.85 | 5.65 | 2.45 |
| Conventional ED | 9.354 | 6.855 | 1.365 | 18.3 | 20.0 | 6.60 | 9.16 |
| Normal PED | 9.395 | 6.832 | 1.375 | 11.5 | 11.7 | 5.00 | 5.50 |
| TS-PED | 9.264 | 6.775 | 1.367 | 14.1 | 14.3 | 5.87 | 5.95 |

**Table 3.** Refined atomic coordinates and thermal parameters obtained from TS-PED data

| Atoms | *x* | *y* | *Z* | *B* (Å$^2$) |
|---|---|---|---|---|
| Ca1 | 2/3 | 1/3 | –0.00402 | 1.65472 |
| Ca2 | –0.01043 | 0.23365 | 0.25 | 1.57127 |
| P | 0.37726 | 0.39858 | 0.25 | 3.51706 |
| O1 | 0.46506 | 0.31919 | 0.25 | 3.49119 |
| O2 | 0.45436 | 0.57942 | 0.25 | 0.36005 |
| O3 | 0.21158 | 0.29793 | 0.09154 | 7.58413 |
| O4 | 0 | 0 | 0.18055 | 17.91892 |
| H | 0 | 0 | 0.06080 (fix) | – |

obtained from ED data depend on the ED calibration for each camera length, while the *a*/*c* ratio of the lattice parameters is more independent of the calibration, which indicates that the accuracy of lattice parameters determined by TS-PED data is superior to that obtained by other ED data. The reliability factors $R_p$, $R_{wp}$ and $\chi^2$ obtained from TS-PED data were 14.1%, 14.3% and 5.95, respectively, which were much better than those from conventional ED data ($R_p$, 18.3%; $R_{wp}$, 20.0%; $\chi^2$, 9.16).

Finally, the refined atomic coordinates together with the thermal parameters *B* (Å$^2$) are presented in Table 3. Although the *R*-factor for structure determination was the best in the result with normal PED data, the atomic coordinates determined by TS-PED data agreed more accurately with the XRD result than those by other ED data (see the supplementary data online Table S1). In addition, the thermal parameters for all atoms were refined more reasonably without negative values in the TS-PED refinement result.

## Discussion

### Electron powder diffraction for structure analysis

In general, nanosized crystalline materials that have various shapes and structures, such as nanopowder, rod, sheet and disk could easily be aggregated and stacked out on the TEM grid. In these cases, it is very difficult to obtain 3D diffraction data from a single nanoparticle owing to sample overlapping during specimen tilting. To overcome this problem, Kolb *et al.* [24–25] recently developed a new ED technique for automatic 3D data acquisition from a single nanoparticle. This technique, however, requires an automation system and a time-consuming procedure to determine the average structure from overall nanocrystallites. On the contrary, the electron powder diffraction of nanopowder allows 3D diffraction data from a number of randomly oriented nanoparticles with the same principle as powder XRD. Because of the stronger interaction of electrons with matter, the acquisition time of ED patterns for 3D diffraction data from small sample amount could drastically be reduced (<30 s), when compared with the XRD method (24 h in our experiment). However, there are practical problems related to the data quality in conventional ED technique, such as intensity ratio, FWHM and usable resolution, which affect reliability of the refined structure.

### Electron beam precession

Incorrect intensity ratio in ED data partly originates from insufficient particle numbers of the illuminating area, which results in discrete diffraction rings due to a lack of their random orientation distribution. In addition, the strong spot intensity taken from the larger crystallites near the zone-axis influences the average intensity of each reflection more severely. The PED technique produces more continuous diffraction rings because more reflections are collected with precession angles (1–3°) for the same illuminating area (same particle numbers), and it minimizes the dynamical effects for the larger crystallites by the beam precession mode (see the supplementary data online Fig. S2). Thus, the results of the PED data have higher uniformity and reliability than those obtained by conventional ED data.

### Theta-scan technique

In our conventional ED results, FWHM values that are related to peak broadening and used as a criterion for data quality were very poor, when compared with those of XRD data as shown in Fig. 3. The FWHM value was even worse in normal PED data against our expectation. In ED application, the 2D area detector is used to acquire ED patterns unlike the point detector in XRD. Therefore, it is very important that the average intensity profiles must be extracted from each ring reflection without any distortion. However, there is a limitation of the descan

alignment of the precession unit. The ring-shaped diffraction beam with a precessed angle must be completely compensated to a stationary focused beam in the descan alignment mode (see the supplementary data online Fig. S3). However, it is extremely difficult to obtain the perfect diffraction data owing to several lens aberrations, namely spherical aberration and 3-fold astigmatism on the TEM. Thus, the peak broadening in polycrystalline ring patterns would be more severe in PED mode than the conventional ED mode [26]. In this study, we applied the TS-PED technique to overcome this problem. As a result, FWHM was improved from 1.18° to 0.61° because of the enhanced pixel resolution, although this value is still higher than that of XRD data. It is expected that the FWHM could be further improved by employing a higher quality detector, such as 4k or higher (8 and 10k) CCD detector or image plate. It is also expected that the peak broadening due to the descan misalignment of the precession unit could be corrected by software compensation in a new digital precession unit 'DigiSTAR' [27], because the software control of the 'DigiSTAR' allows better focalization of the primary and diffracted electron beam during the scan and descan process of beam precession.

### Useable ED resolution

Another consideration is the usable data resolution for structure determination by electron powder diffraction. Although we had collected ED data with a resolution of 0.7 Å, we used the resolution of 0.9 Å in our best refinement result while that of XRD data was 0.8 Å. For this reason, Cascarano *et al.* [28] recently reported that the difference in atomic scattering power between electron and X-ray should be considered for structure analysis using ED. The atomic scattering curve for ED decreases more rapidly with scattering vector (**s**) than the corresponding X-ray curves. Therefore, the measurement errors in higher scattering angle (higher resolution data) are expected to be larger than those of XRD. In this respect, our best refinement results (used data resolution) could have been possibly influenced by the characteristic of atomic scattering power in electrons.

## Conclusion

In this study, we evaluated the usefulness of TS-PED technique for structure analysis of the HA nanopowder. The average intensity profiles of electron powder diffraction were collected more reliably by TS-PED owing to the precession effect and higher peak resolution. When compared with conventional ED results, the structural reliability refined by applying TS-PED was improved significantly in spite of small numbers of nanopowder and the drawbacks of our precession unit.

Finally, it was demonstrated that TS-PED technique could be a useful analytical method for structure determination utilizing electron powder diffraction. TS-PED could be an alternative solution to overcome the limitations of XRD and conventional ED for the study of nanosized crystalline materials, especially when combined with a digitalized precession unit and energy-filtering function.

## Supplementary data

Supplementary data are available at http://jmicro.oxfordjournals.org/.

## Acknowledgement

We appreciate Dr Deok Kyo Lee of National Fusion Research Institute, South Korea, for his kind review of our manuscript.

## Funding

This work was supported by KBSI (Korea Basic Science Institute) grant (T31801) to J.-G.K.

## References

1 Weirich T E, Winterer M, Seifried S, Hahn H, and Fuess H (2000) Rietveld analysis of electron powder diffraction data from nanocrystalline anatase, $TiO_2$. *Ultramicroscopy* **81**: 263–270.

2 Kim J-G, Seo J W, Cheon J, and Kim Y-J (2009) Rietveld analysis of nano-crystalline $MnFe_2O_4$ with electron powder diffraction. *Bull. Korean Chem. Soc.* **30**: 183–187.

3 Weirich T E, Winterer M, Seifried S, and Mayer J (2002) Structure of nanocrystalline anatase solved and refined from electron powder data. *Acta Crystallogr. A* **58**: 308–315.

4 Vincent R and Midgley P A (1994) Double conical beam-rocking system for measurement of integrated electron diffraction intensities. *Ultramicroscopy* **53**: 271–282.

5 Dorset D L, Gilmore C J, Jorda J L, and Nicolopoulos S (2007) Direct electron crystallographic determination of zeolite zonal structures. *Ultramicroscopy* **107**: 462–473.

6 Gemmi M and Nicolopoulos S (2007) Structure solution with three-dimensional sets of precessed electron diffraction intensities. *Ultramicroscopy* **107**: 483–494.

7 Berg B S, Hansen V, Midgley P A, and Gjønnes J (1998) Measurement of three-dimensional intensity data in electron diffraction by the precession technique. *Ultramicroscopy* **74**: 147–157.

8 Boulahya K, Ruiz-González L, Parras M, González-Clabet J M, Nickolsky M S, and Nicolopoulos S (2007) *Ab initio* determination of heavy oxide perovskite related structures from precession electron diffraction data. *Ultramicroscopy* **107**: 445–452.

9 Nicolopoulos S, Morniroli J P, and Gemmi M (2007) From powder diffraction to structure resolution of nanocrystals by precession electron diffraction. Z. *Kristallogr.* Suppl. **26**: 183–188.

10 Kim J-G, Song K, Kwon K, Hong K, and Kim Y-J (2010) Structure analysis of inorganic crystals by energy-filtered precession electron diffraction. *J. Electron Microsc.* **59**: 273–283.

11 Weirich T E, Portillo J, Cox G, Hibst H, and Nicolopoulos S (2006) *Ab initio* determination of the framework structure of the heavy-metal oxide $Cs_xNb_{2.54}W_{2.46}O_{14}$ from 100 kV precession electron diffraction data. *Ultramicroscopy* **106**: 164–175.

12 Prodan G and Ciupina V (2010) Rietveld analysis of polycrystalline materials using precession of electron diffraction. *Rom. Biotechnol. Lett.* **15**: 102–108.

13 Jevti M, Mitri M, Škapin S, Janar B, Ignjatovi N, and Uskokovi D (2008) Crystal structure of hydroxyapatite nanorods synthesized by sonochemical homogeneous precipitation. *Cryst. Growth Design* **8**: 2217–2222.

14 Wei J, Li Y, Chen W, and Zuo Y (2003) A study on nano-composite of hydroxyapatite and polyamide. *J. Mater. Sci.* **38**: 3303–3306.

15 Hughes J M, Cameron M, and Crowley K D (1989) Structural variation in natural F, OH, and Cl apatites. *Am. Mineral.* **74**: 870–876.

16 Zou X D, Sukharev Y, and Hovmöller S (1993) ELD – a computer program system for extracting intensities from electron diffraction patterns. *Ultramicroscopy* **49**: 147–158.

17 Rodriguez-Carvajal J (2000) *FULLPROF – a program for Rietveld, profile matching and integrated intensities refinement of X-ray and/or neutron data* (Laboratoire Leon Brillouin: CEA-Saclay, France).

18 Rietveld H M (1967) Line profiles of neutron powder-diffraction peaks for structure refinement. *Acta Crystallogr.* **22**: 151–152.

19 Larson A C and Von Dreele R B (2004) General structure analysis system (GSAS). Los Alamos National Lab. Report LAUR 86–748.

20 Olszta M J, Cheng X, Jee S S, Kumar R, Kim Y-Y, Kaufman M J, Douglas E P, and Gower L B (2007) Bone structure and formation: a new perspective. *Mater. Sci. Eng.* **R58**: 77–116.

21 Wenk H R and Heidelbach F (1999) Crystal alignment of carbonated apatite in bone and calcified tendon: results from quantitative texture analysis. *Bone* **24**: 361–369.

22 Su X, Sun K, Cui F Z, and Landis W J (2003) Organization of apatite crystals in human woven bone. *Bone* **32**: 150–162.

23 Jiang J S and Li F H (1984) Fitting the atomic scattering factors for electrons to an analytical formula. *Acta Phys. Sin.* **33**: 846–849.

24 Kolb U, Gorelik T, Kübel C, Otten M T, and Hubert D (2008) Towards automated diffraction tomography. Part I. Data acquisition. *Ultramicroscopy* **107**: 507–513.

25 Kolb U, Gorelik T, and Otten M T (2008) Towards automated diffraction tomography. Part II. Cell parameter determination. *Ultramicroscopy* **108**: 763–772.

26 Own C S, Sinkler W, and Marks L D (2007) Prospects for aberration corrected electron precession. *Ultramicroscopy* **107**: 534–542.

27 Portillo J, Rauch E F, Nicolopoulos S, Gemmi M, and Bultrys D (2010) Precession electron diffraction assisted orientation mapping in the transmission electron microscope. *Mater. Sci. Forum* **644**: 1–7.

28 Cascarano G L, Giacovazzo C, and Carrozzini B (2010) Crystal structure solution via PED data: the BEA algorithm. *Ultramicroscopy* **111**: 56–61.